Int. J. Heat Mass Transfer. Vol. 28, No. 7, pp. 1293–1305, 1985
Printed in Great Britain

0017-9310/85 $3.00 + 0.00

An investigation of laminar mixed convection inside a horizontal tube with isothermal wall conditions

J. PASCAL COUTIER
Passive Research and Development, Lawrence Berkeley Laboratory, Berkeley, CA 94720, U.S.A.

and

RALPH GREIF
Mechanical Engineering Department, University of California, Berkeley, CA 94720, U.S.A.

(*Received* 20 *August* 1984 *and in final form* 11 *December* 1984)

Abstract—The laminar flow and heat transfer within a horizontal isothermal tube are studied both experimentally and theoretically. Emphasis is given to flow regimes where a buoyant effect on the forced flow is exhibited within the tube. Several tests were carried out over a wide range of operating conditions with water and a propylene–glycol solution inside the tube. A three-dimensional numerical model was used to analyze the flow behavior and the heat transfer. The secondary flows create a large circumferential variation of the fluid temperature and the Nusselt number.

INTRODUCTION

THE PRESENT work is a study of laminar convection inside a horizontal tube, including the effect of buoyancy on heat transfer and fluid motion. In a horizontal tube, the buoyancy arises in a plane perpendicular to the direction of fluid motion and results from the temperature difference between the wall and the bulk fluid. The hot fluid located near the tube axis rises due to buoyant forces and as it reaches the wall, cools and then flows down along the sides of the tube. This secondary flow combined with the main axial motion creates a spiraling effect which has a strong influence on the heat transfer. Among the typical boundary conditions studied for the tube, the constant heat flux condition has been widely investigated. The isothermal wall condition has received less attention, with the primary emphasis on obtaining Nusselt number correlations. When the tube wall is maintained at a constant temperature, the natural convection effects diminish as the fluid proceeds downstream.

Correlations for the Nusselt number with the isothermal wall boundary condition have been obtained from experimental results by Sieder and Tate [1], Brown and Thomas [2], Kern and Othmer [3], Oliver [4] and by Depew and August [5]. Recently Hieber [6] attempted to include all previous experimental results into a new equation with a different format. Numerical studies of the problem under isothermal wall condition were carried out by Ou and Cheng [7], by Hieber and Sreenivasan [8] and Hieber [9]. Both methods yielded results which compared well with the experimental data. Ou and Cheng used the large Prandtl number assumption to solve the conservation equations and obtained fair agreement with the existing correlations for the rate of heat transfer. Hieber and Sreenivasan [8] divided the tube length into five zones to study the various phases of the secondary flow development. Proof that the large Prandtl number assumption was valid for values of Pr close to unity was also given in that study which achieved satisfactory results for the heat transfer. The extensive work which has been carried out for the constant wall heat flux condition, particularly on the experimental validation of the various models developed for solving the problem, is described in refs. [10–21].

The purpose of this paper is to give a detailed analysis of the phenomena encountered under isothermal wall conditions. Experimental testing and numerical calculations were carried out to evaluate the effects of buoyancy on the fluid flow and heat transfer rate over a wide range of operating conditions.

THE EXPERIMENTAL STUDY

The test facility shown in Fig. 1 was a full-scale system which had been designed to evaluate the performance of solar thermosiphons with heat exchangers. The apparatus was modified to accommodate more refined temperature measurements, particularly inside the heat exchanger tube.

The main features of the system are:

(1) Two solar collectors with a total glazing area of 3.47 m^2 with long strip heaters attached to the rear of the absorber plates.
(2) A cylindrical storage tank, made of steel, 1.52 m long and 0.51 m in diameter, wrapped with a 0.1-m-thick layer of foam glass insulation.
(3) Collector to tank piping made of 2.5-cm-I.D. silicone hose, insulated with a 1.8-cm-thick elastomeric foam.
(4) A heat exchanger made of two copper tubes, each

NOMENCLATURE

A	aspect ratio
A'	characteristic velocity, $[gr_0/(T(r,\phi,z)-T_w)]^{1/2}$
a_{nb}	diffusion and convection coefficient
c_p	heat capacity at constant pressure [J kg^{-1} K^{-1}]
d	heat exchanger inside tube diameter [m]
$\mathbf{F}$	body force vector
$\mathbf{g}$	acceleration vector
g	acceleration due to gravity [m s^{-2}]
Gr	Grashof number, $\beta g d^3(T-T_w)\rho^2/\mu^2$
Gz	Graetz number, $RePr\pi d/4L$
h	height above a datum [m]
h'	convective heat transfer coefficient [W m^{-2} K^{-1}]
k	conductivity [W m^{-1} K^{-1}]
L	heat exchanger tube length [m]
m	mass flow-rate [kg s^{-1}]
Nu	Nusselt number, $h'd/k$
$Nu(\phi,z)$	local Nusselt number, function of ϕ and z
$\overline{Nu}(z)$	average local Nusselt number, function of z
$\overline{Nu}$	average Nusselt number
p	pressure [Pa]
p	thermodynamic pressure [Pa]
P	dimensionless pressure, $p/\rho v_m^2$
Pr	Prandtl number, $c_p\mu/k$
r	radial coordinate
r_0	tube radius [m]
Ra	inner flow Rayleigh number, $Pr\,\beta\rho^2 g d^3(T-T_w)/\mu^2$
Re	Reynolds number, $\rho v_m d/\mu$
S	source term
T	temperature [°C]
T_{in}	inlet temperature [°C]
T_{out}	outlet temperature [°C]
T_w	wall temperature [°C]
$\mathbf{u}$	velocity vector
u	radial component of the velocity
U	dimensionless radial velocity
v	circumferential component of the velocity
v_m	mean axial velocity
v_s	average cross-sectional velocity
V	dimensionless circumferential velocity
W	dimensionless axial velocity
z	axial component
Z	dimensionless axial coordinate.

Greek symbols

α	thermal diffusivity [m^2 s^{-1}]
β	coefficient of thermal expansion [K^{-1}]
Γ	diffusion coefficient
ε	dimensionless temperature gradient, $\beta(T-T_w)$
η	dimensionless radial coordinate
θ	dimensionless temperature, $(T-T_w)/(T_{in}-T_w)$
μ	dynamic viscosity [Pa s]
μ_w	dynamic viscosity at the wall [Pa s]
ν	kinematic viscosity [m^2 s^{-1}]
ρ	density [kg m^{-3}]
ρ_w	density at the wall [kg m^{-3}]
ϕ	angular coordinate
ψ	any dependent variable in the code.

Subscripts

b	bulk
in	inlet
out	outlet
w	wall.

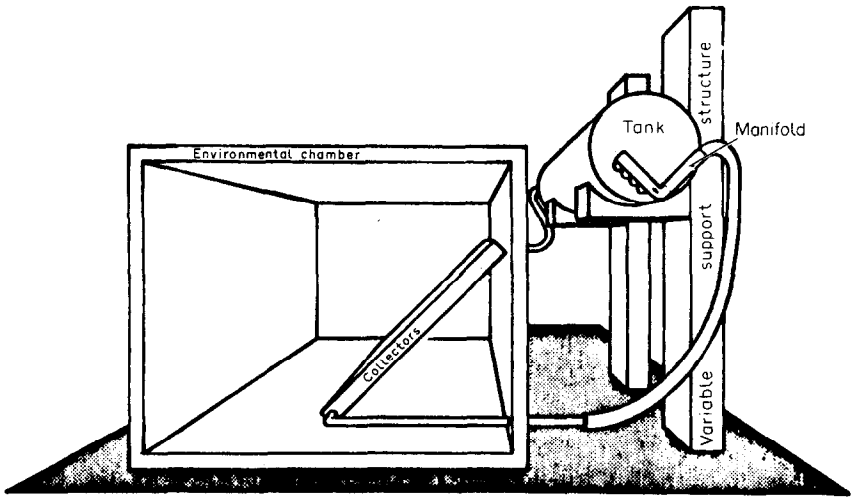

FIG. 1. Schematic of the test facility.

with an O.D. of 2.54 cm, wall thickness of 0.3 cm and length of 1.52 m. The two tubes were placed 0.35 m apart, parallel to the tank axis.

The loop was comprised of the collectors, the piping and the heat exchanger tube, and the fluid was circulated through the system by a small 1/8 h.p. pump. The flow-rate was measured using a positive displacement flow-meter which was coupled to a pulse counter. Heat was added to the system from the strip heaters attached to the absorber plates of the solar collectors. The heat input was controlled by a burst firing SCR power controller.

The heat exchanger loop contained about 18 dm^3 of fluid, which was either water or a solution (60% by weight) of propylene–glycol. The storage tank had a capacity of 300 dm^3 of water.

All temperatures were measured using copper–constantan thermocouples. Two types of coatings, Teflon and plastic, were used and the thermocouples used at the inlet and outlet of the heat exchanger tube were sheathed to allow them to be pushed through rubber-sealed fittings. Twenty-four thermocouples were located at three equally-spaced axial locations in the storage tank to permit a detailed evaluation of the water temperature surrounding the heat exchanger tube. Four axial locations were chosen along the tube ($L/12$, $L/6$, $L/2$, $5L/6$) to record the fluid and wall temperatures (cf. Fig. 2). The last three locations coincided with the tank temperature grids, and the first location was added to provide additional information on the thermal boundary layer.

To minimize the disturbance to the flow, the thermocouples used to measure the heat exchanger fluid temperatures were small, 2 mm in diameter. The inlet and outlet temperatures for the heat exchanger tube were measured with the sheathed thermocouples noted above. For most of the experiments, the tips of these probes were located on the tube center line. At each of the four axial locations where the tube temperature was measured, five probes were used. Two of them recorded the fluid temperatures at the tube center line and at two-thirds of the radius at an angle ϕ equal to 0° (cf. Fig. 3). Three wall temperatures were also measured using wall temperature probes constructed by Omega Engineering, Inc. They were located on the north, east and south sides of the wall (when facing downstream), whereas the fluid temperature probes were inserted through a sealed hole on the west side of the tube as shown in Fig. 3. Only one of the two tubes was equipped with these probes, but one thermocouple was placed on the other tube at the same axial location as that for the tube studied, so that symmetry could be checked. A long piece of well-insulated pipe of the same diameter as the heat exchanger tube preceded the entrance to the tube, ensuring that a fully developed velocity profile was a good assumption for inlet conditions. In addition, measurements showed that the inlet temperature did not vary along the tube diameter, which enabled the use of constant temperature inlet condition in the numerical analysis.

Each test was run for a period varying from 10 to 24 h under constant heat input conditions. Steady-state conditions were attained after 2–3 h and were maintained for the remainder of the test. Constant wall temperature was achieved by constantly replacing the water near the outside tube wall through the use of a circulating pump for the storage water. A small mixing pump was also used to minimize stratification above the tubes. The axial velocity of the water circulating near the tube wall was estimated to be about 1 mm s^{-1}, which is small enough to neglect convective effects at the outer surface of the tube wall. The city water used to cool the tube was at a fairly constant temperature over

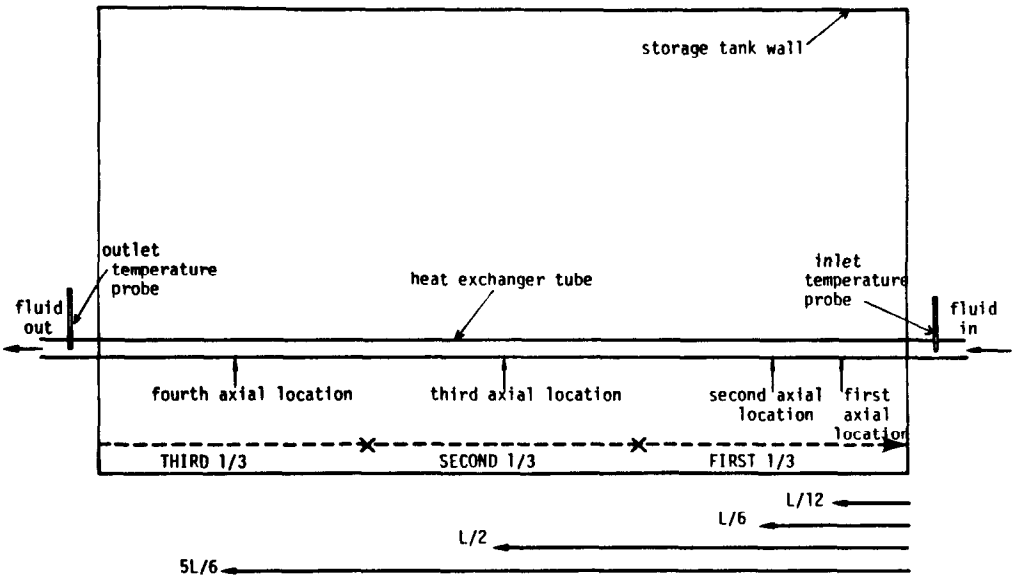

FIG. 2. Schematic of the heat exchanger-tube.

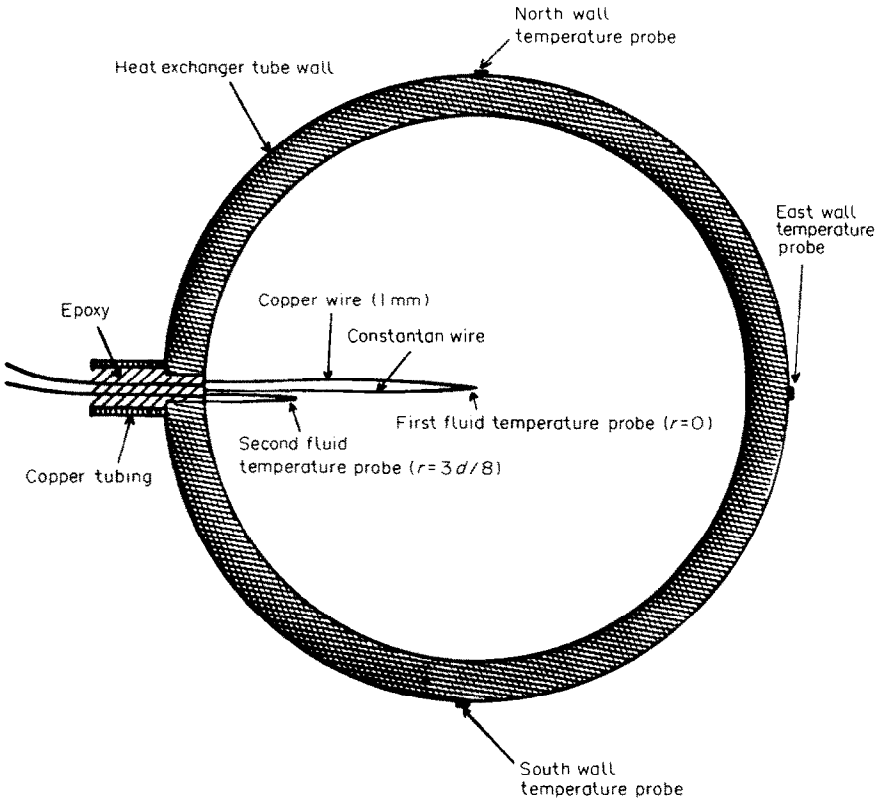

FIG. 3. Cross-section of the heat exchanger tube with location of the temperature probes.

the entire test time (less than 0.5°C variation over a 24-h period). A wide range of operating conditions was covered by varying the power input and the flow-rate. Table 1 summarizes the conditions used in each test.

Flow visualization was performed to substantiate the assumption that the secondary flow effects were important. The facility was modified to allow direct viewing of the flow. Since it was not possible to see the flow inside the storage tank itself, visualization was carried out at the outlet of the heat exchanger tube. A red dye solution (layout dye by Dykem, No. dx-296) was chosen for its density (1002 kg m^{-3} at 20°C) which was very close to that of water.

A 90° elbow transparent fitting which allowed cross-sectional viewing of the flow was constructed from Plexiglass. Its clear and flat window was the same size as that of the tube, which permitted a direct view of the flow with negligible visual distortion. An additional 15-cm-long piece of transparent pipe was inserted before the fitting to provide natural lighting within the pipe.

The dye solution was pre-heated to a temperature close to the outlet temperature of the heat exchanger fluid. This temperature was generally 20°C above the wall temperature inside the tank and approx. 15°C above the transparent pipe wall (exposed to ambient air conditions). The tip of the syringe used to inject the dye was placed at the tube center line and was constructed such that the dye was introduced in large drops (about 3 mm in diameter) with negligible momentum. The dye mixed with the water and travelled downstream toward

Table 1. Operating conditions for the seven cases studied

Case No.	1	2	3	4	5	6	7
Fluid	water	water	water	water	water	glycol	glycol
Flow-rate ($dm^3\ mm^{-1}$)	0.753	2.015	1.210	0.810	0.378	0.497	0.746
Average axial velocity ($cm\ s^{-1}$)	1.644	4.398	1.085	1.767	0.822	1.085	1.627
Inlet temperature (°C)	38.3	32.2	40.7	34.7	59.3	40.7	60.5
Wall temperature (°C)	15.7	15.5	16.8	25.6	15.6	16.8	15.7
Re	454	1160	298	508	270	40	104
$Ra \times 10^6$	3.9	3.2	3.5	1.8	9.0	1.6	5.5
Pr	5.35	5.65	5.40	5.15	4.4	46.0	28.1
Gr/Re^2	3.53	0.42	7.30	1.37	28.05	22.41	18.10

the transparent fitting. The axial velocity was adjusted using throttling valves such that the travel time was approx. 20 s. Photographs were taken every 2 s and focused on the center of the transparent pipe. This experiment was repeated several times for various conditions.

THE NUMERICAL MODEL

The presence of the secondary flow requires that a three-dimensional analysis be carried out. The presence of buoyant forces means that the momentum and the energy equations must be solved simultaneously.

In this study, the following assumptions have been made:

(1) steady-state conditions;
(2) laminar flow;
(3) incompressible fluid;
(4) negligible viscous dissipation; and
(5) constant physical properties, except for the density.

All the physical properties in the model were taken at a temperature of 25°C. The Boussinesq approximation was used, which specifies the density to be a constant everywhere except in the body force term of the momentum equation, where it is assumed to vary linearly with temperature. The following expression has been assumed for the density:

$$\rho = \rho_w[1-\beta(T-T_w)]. \tag{1}$$

The conservation equations can be written as follows:

$$\text{Continuity}: \nabla\cdot\mathbf{u} = 0 \tag{2}$$

$$\text{Momentum}: \rho\mathbf{u}\cdot\nabla\mathbf{u} = \mathbf{F}-\nabla\hat{p}+\mu\nabla\cdot\nabla\mathbf{u} \tag{3}$$

$$\text{Energy}: \rho c\mathbf{u}\cdot\nabla T = k\nabla\cdot\nabla T. \tag{4}$$

A simplification can be made to the momentum equation by introducing a new pressure variable:

$$\hat{p} = p+\rho_w g h \tag{5}$$

where h is the height above a datum plane. The quantity $\mathbf{F}-\nabla\hat{p}$ is written as follows:

$$\mathbf{F}-\nabla\hat{p} = \rho g-\nabla p-\rho_w g = -\nabla p-\rho_w g\beta(T-T_w). \tag{6}$$

The momentum equation then becomes:

$$\rho_w\mathbf{u}\cdot\nabla\mathbf{u} = -\nabla p-\rho_w\beta(T-T_w)g+\mu\nabla\cdot\nabla\mathbf{u}. \tag{7}$$

For the present problem, the cylindrical coordinate system was used, where ϕ is the angle around the pipe, r is the radial coordinate and z is the axial coordinate (cf. Fig. 4). The boundary conditions for this problem are:

(1) $u(r,\phi,z=0) = v(r,\phi,z=0) = 0$ (no secondary flow at the entrance to the heat exchanger tube)
(2) $w(r,\phi,z=0) = 2v_m/(1-r^2/r_0^2)$
(3) $T(r,\phi,z=0) = T_{in}$ = constant
(4) $u(r=r_0,\phi,z) = v(r=r_0,\phi,z) = w(r=r_0,\phi,z) = 0$

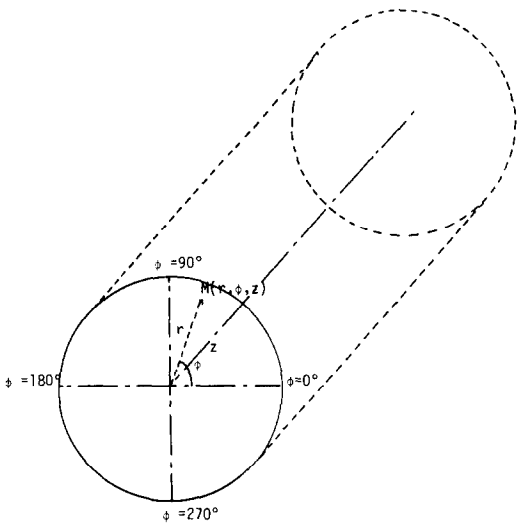

FIG. 4. Coordinate system.

(5) $u(r=0,\phi,z), v(r=0,\phi,z), w(r=0,\phi,z)$ and $T(r=0,\phi,z)$ finite
(6) symmetry about a vertical plane: for example, $u(r,\phi,z) = u(r,-\phi,z)$
(7) $T(r=r_0,\phi,z) = T_w$ = constant.

A dimensionless form of the conservation equations can be written (cf. ref. [13]) to yield:

conservation of mass:

$$\frac{\partial U}{\partial\eta}+\frac{U}{\eta}+\frac{1}{\eta}\frac{\partial V}{\partial\Phi}+\frac{\partial W}{\partial Z} = 0 \tag{8}$$

conservation of momentum:

r-direction:

$$\frac{Gr}{Re^2}\left[\frac{\partial U}{\partial\eta}+\frac{V}{\eta}\frac{\partial U}{\partial\Phi}-\frac{V^2}{\eta}+W\frac{\partial U}{\partial Z}\right] = -\frac{\partial P}{\partial\eta}-\frac{Gr}{Re^2}\theta\sin\phi+\frac{Gr}{Re^2(Gr)^{1/2}}\times\left[\frac{\partial}{\partial\eta}\left(\frac{1}{\eta}\frac{\partial}{\partial\eta}(\eta U)\right)+\frac{1}{\eta^2}\frac{\partial^2 U}{\partial\Phi^2}+\frac{\partial^2 U}{\partial Z^2}-\frac{2}{\eta^2}\frac{\partial V}{\partial\phi}\right] \tag{9}$$

ϕ-direction:

$$\frac{Gr}{Re^2}\left[\frac{\partial V}{\partial\eta}+\frac{V}{\eta}\frac{\partial V}{\partial\Phi}+\frac{UV}{\eta}+W\frac{\partial V}{\partial Z}\right] = -\frac{\partial P}{\eta\,\partial\Phi}+\frac{Gr}{Re^2}\theta\cos\phi+\frac{Gr}{Re^2(Gr)^{1/2}}\times\left[\frac{\partial}{\partial\eta}\left(\frac{1}{\eta}\frac{\partial}{\partial\eta}(\eta V)\right)+\frac{1}{\eta^2}\frac{\partial^2 V}{\partial\Phi^2}+\frac{\partial^2 V}{\partial Z^2}+\frac{2}{\eta^2}\frac{\partial U}{\partial\phi}\right] \tag{10}$$

z-direction:

$$U\frac{\partial W}{\partial\eta}+\frac{V}{\eta}\frac{\partial W}{\partial\Phi}+W\frac{\partial W}{\partial Z} = -\frac{d}{L}\frac{\partial p}{\partial Z}\left(\frac{Gr}{Re^2}\right)^{-1/2}+\frac{1}{Gr^{1/2}}\left[\frac{1}{\eta}\frac{\partial}{\partial\eta}\left(\eta\frac{\partial W}{\partial\eta}\right)+\frac{1}{\eta^2}\frac{\partial^2 W}{\partial\phi^2}+\frac{\partial^2\theta}{\partial Z^2}\right] \tag{11}$$

conservation of energy:

$$U\frac{\partial\theta}{\partial\eta}+\frac{V}{\eta}\frac{\partial\theta}{\partial\Phi}+W\frac{\partial\theta}{\partial Z}=\frac{1}{Pr(Gr)^{1/2}}\times\left[\frac{1}{\eta}\frac{\partial}{\partial\eta}\left(\eta\frac{\partial\theta}{\partial\eta}\right)+\frac{1}{\eta^2}\frac{\partial^2\theta}{\partial\phi^2}+\frac{\partial^2\theta}{\partial Z^2}\right]. \quad (12)$$

The ratio Gr/Re^2 is a characteristic quantity for this problem.

The program used to carry out the calculation was TOROID, a three-dimensional version of the program TEACH [22] adapted to toroidal coordinates. The code solved the elliptic forms of the conservation equations in terms of a finite difference formulation as described by Humphrey in [23] and Patankar [24]. The methodology used for solving the set of equations is described in Appendix B and by Humphrey [23] and Lavine [25].

RESULTS AND DISCUSSION

(A) *Flow visualization*

The following description of the secondary flow patterns comes from experimental conditions with the following characteristics:

(1) The ratio Gr/Re^2 was about 8, which indicated strong buoyant forces.

(2) The ratio v_s/v_m, calculated at the end of the chapter, reached values of 0.2 to 0.3, where v_s is the mean velocity component in the tube cross-section, and v_m is the mean axial component.

Dye was injected at the center of the tube cross-section and rose quickly to the top of the tube, showing that significant buoyant forces exist. The dye diffuses and forms a cloud, which then flows down along the two sides. Due to the slow axial motion of the fluid near the wall, this cloud of red dye lingers near the wall. As the front edge of the dye reaches a location at approximately 220° (or 320° on the other side of the vertical symmetry axis, cf. Fig. 4), its motion is significantly altered and the cloud moves back toward the center of the cross-section. At that axial location, the fluid has travelled through the transparent portion of the pipe, and further observation is not possible. The symmetry of the motion about the vertical line was demonstrated by two identical clouds moving in each half of the tube cross-section. A more detailed description of visual observations, supported by color photographs, is given in ref. [26].

(B) *Temperature distribution*

Figures 5 and 6 present the experimental and numerical results for the axial variation of the temperature for cases 1 and 5 (cf. Table 1) for which

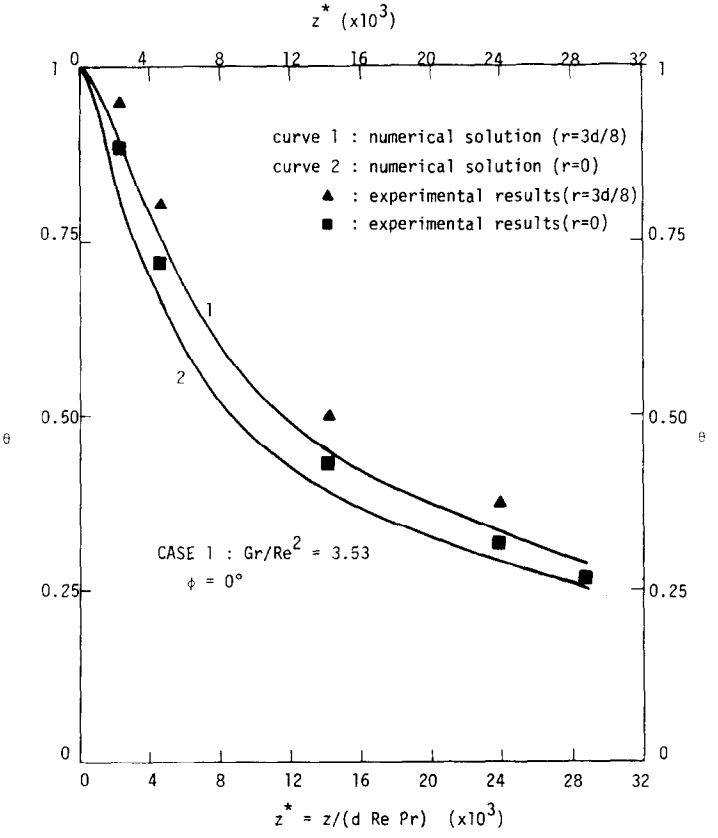

FIG. 5. Dimensionless temperature axial variation: Case 1 (BC 1; $Ra = 3.9 \times 10^6$; $Re = 454$).

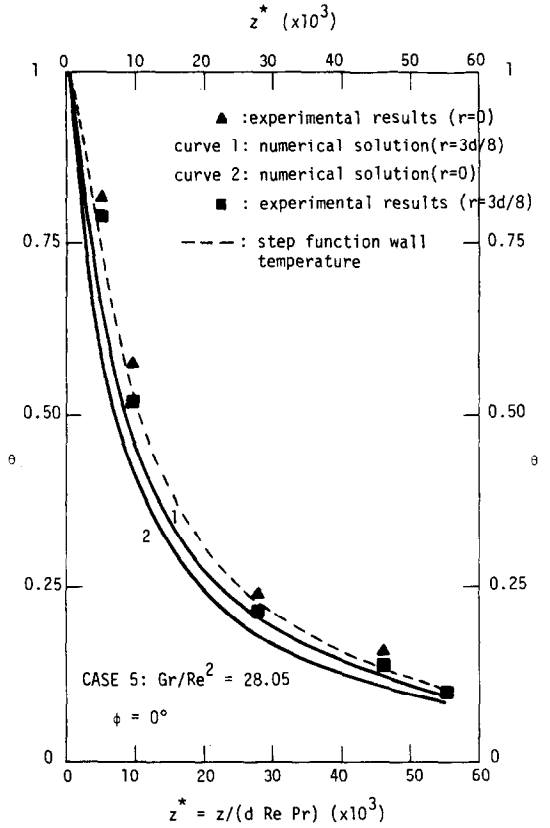

FIG. 6. Dimensionless temperature axial variation: Case 5 (BC 1; $Ra = 9.0 \times 10^6$; $Re = 270$).

water was the test fluid. All curves are for the angular position $\phi = 0°$. Figure 5 shows a larger temperature at $r = 3d/8$ than for $r = 0$. This is a consequence of the presence of the secondary flow and is discussed in Section D. All the tests exhibit a large decrease in the temperature near the entrance, because of the large temperature difference between the fluid and the wall. As the fluid progresses downstream toward the tube outlet, the axial temperature variations at both radial locations follow a similar trend. This is consistent with the diminution in the buoyant force, due to the smaller temperature difference between the fluid and the wall. Since the temperature profile for forced, non-buoyant flow predicts a monotonic radial variation for the temperature (the temperature being maximum at the tube centerline), it is expected that these curves will cross as z increases (i.e. as buoyancy becomes less important), particularly over the lower half of the tube cross-section ($270° < \phi < 0°$) where buoyant effects are smaller. The disagreement between predicted and measured values generally varies between 3 and 10% (depending on the axial and radial locations), except for test 5 (cf. Fig. 6) for which the first two axial locations exhibit a larger differential (close to 20%).

Almost all of the predicted values are below the experimental data points. This suggests a systematic error which may be related to the 'constant wall temperature' condition. As stated earlier, cooling fluid at constant temperature flowed past the outer wall of the heat exchanger and the measured wall temperature decreased slightly downstream. The largest decrease in the wall temperature between the first and last locations was 3.5°C for an initial fluid-to-wall difference of 44°C (test 5). The angular variation of the wall temperature was generally very small (less than 0.3°C throughout the tube length). The constant value of the wall temperature used in the program was the value at the middle of the tube length. Near the tube entrance, the wall temperature was somewhat larger (1 to 2°C) than at the middle of the length. Experimentally, the wall temperature variation over the second half of the tube was found to be negligible.

Figure 6 also shows a dotted curve which represents the calculated profile for a wall temperature variation which is in better agreement with the measured values. For this calculation, instead of assuming a constant wall temperature throughout the tube axis length, the wall temperature was specified by using a series of step functions which more closely fit the experimentally recorded wall temperatures. The resulting good agreement leads to the conclusion that the systematic error found earlier is primarily due to the slight experimental variation of the wall temperature.

Figure 7 shows the radial temperature profiles at several axial positions for the angular position $\phi = 0°$. The temperature profile calculated for forced flow with no buoyant forces is also shown. The agreement between the experimental data and the theoretical values is very good. For this angular location, the profiles appear to peak near $r = 7d/16$. Figure 8 demonstrates that the non-monotonic profiles are found for the upper half of the tube cross-section ($0° < \phi < 180°$) whereas the lower half exhibits a monotonic variation. Since the non-monotonic profile results from the strong buoyant effects (cf. section D), it appears that the secondary flow effects on the temperature profile occur mostly in the top half of the tube.

(C) *Heat transfer results*

Numerically determined values of the Nusselt number are reported in Fig. 9, which shows the axial variation of the local Nusselt number defined by:

$$Nu(z, \phi) = -\frac{1}{d}(\partial T(r, \phi, z)/\partial r, \text{ at } r = d/2)/(T_b(z) - T_w)$$

where:

$$T_b(z) = \left[\int_0^{\pi}\int_0^{d/2} \rho w(r, \phi, z) T(r, \phi, z)\, dr\, d\phi\right] \div \left[\int_0^{\pi}\int_0^{d/2} \rho w(r, \phi, z)\, dr\, d\phi\right].$$

Results are given for ϕ-values of 80° and 280° to avoid presenting profiles on the vertical diameter which is a symmetry line for the secondary flow patterns. Figure 9 displays the following characteristics:

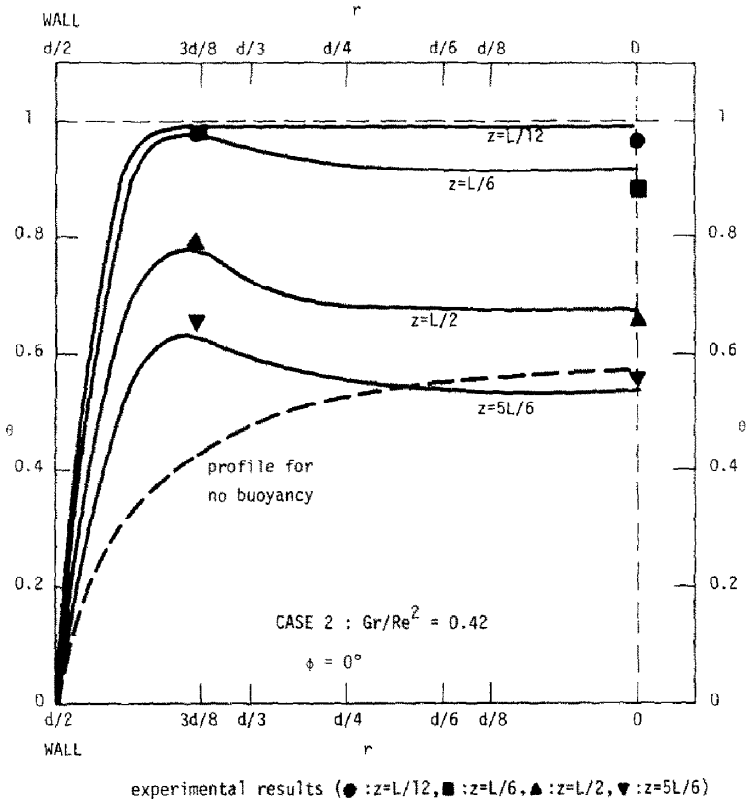

FIG. 7. Dimensionless temperature radial variation: Case 2 (BC 1; $Ra = 3.2 \times 10^6$; $Re = 1160$).

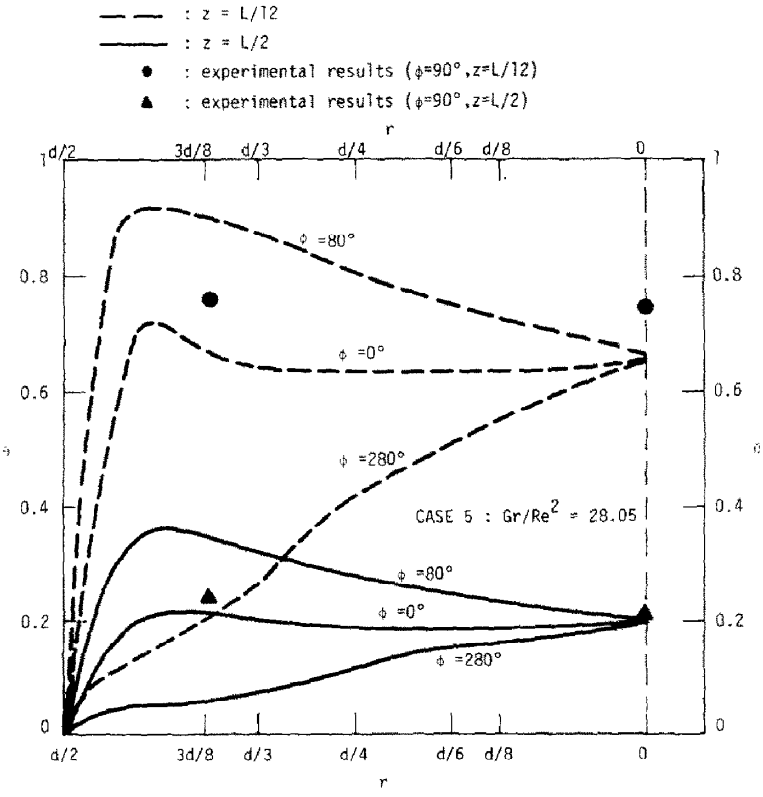

FIG. 8. Dimensionless temperature radial variation: Case 5 (BC 1; $Ra = 9.0 \times 10^6$; $Re = 104$).

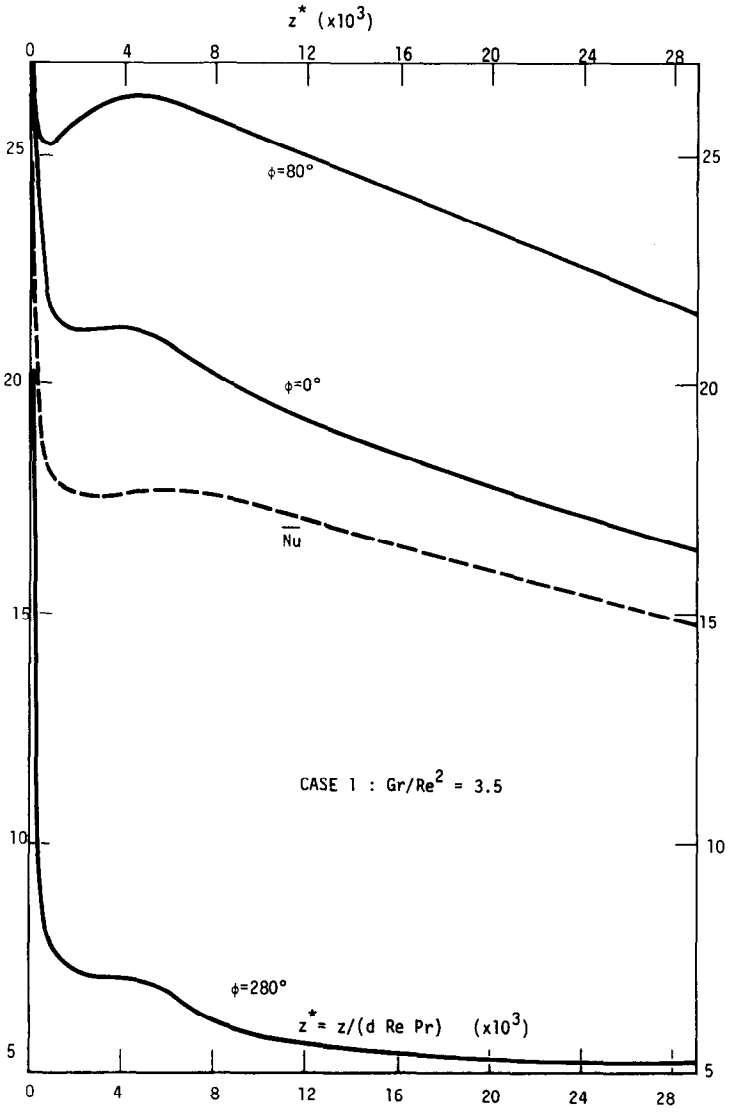

FIG. 9. Local and average Nusselt number axial variation: Case 1 (BC 1; $Ra = 3.9 \times 10^6$; $Re = 454$).

(1) The Nusselt number is maximal near the top of the tube where the hot buoyant stream of fluid first comes in contact with the cold wall.

(2) For most cases, the variation of the Nusselt number with respect to axial distance is not monotonic. As the fluid progresses downstream, it acquires a spiraling motion which brings the hot fluid, first located near the center line, into the upper half of the tube cross-section. This developing secondary flow effect results in the small increase of the heat transfer seen on Figure 9 at $\phi = 280°$.

(3) The gap between the curves $\phi = 280°$ and 0° is much larger than that between the curves $\phi = 0°$ and 80°. The cooling is most effective near the top of the tube where the heat transfer is a maximum. As the fluid flows down and cools along the side wall, the fluid exchanges less heat with the wall and the value of the Nusselt number decreases. In Fig. 9, the dotted curve represents the 'average cross-sectional' Nusselt number obtained by averaging 11 values of the local number at angles between $\phi = 270°$ and $\phi = 90°$.

The aspect ratio (length to diameter) of the heat exchanger tube is $A = L/d = 69$. The value of the average Nusselt number obtained for fully-developed flow under the isothermal wall condition ($Nu = 3.658$) was not attained for any of the seven cases analyzed. Table 2 shows the comparison at the tube outlet between the calculated value of the Nusselt number and the results obtained from earlier correlations [5–7]. Considerable discrepancies are found between the results obtained for the selected correlations. For water, the best agreement is found with the correlation proposed by Depew and August. However, when glycol is considered, Hieber's correlation gives the best result.

(D) *Other results*

The left side of Figs. 10 and 11 shows the calculated streamlines which clearly depict the secondary flow

Table 2. Comparison between calculated Nusselt number and values derived from existing correlations

Case No.	1	2	3	4	5	6	7
Fluid	water	water	water	water	water	glycol	glycol
Calculated *Nu*	8.8	12.6	6.8	9.2	7.3	8.7	11.8
Nu Hieber [6]	11.6	17.0	10.4	10.7	9.9	9.0	11.9
Nu Depew and August [5]	10.0	13.5	8.9	10.0	8.6	8.3	9.9
Nu Oliver [4]	13.3	16.2	13.7	11.7	15.6	12.2	14.3

circulation. For the smaller value of the ratio Gr/Re^2 in Fig. 10, the point of maximum value of the stream function is slightly below the horizontal line ($\phi = 0°$ and 180°), indicating a fairly weak secondary flow effect. The variation of the isotherms is shown on the right side of Figs. 10 and 11. The isothermal curves are very closely spaced except in the bottom region of the tube.

The streamlines in Fig. 10 are almost symmetric about the horizontal diameter at $\phi = 0°$. For larger values of the quantity Gr/Re^2 (cf. Fig. 11), the streamlines follow a similar pattern with two exceptions:

(1) the streamlines are now tilted about 30° clockwise with respect to a vertical line.
(2) the location of the maximum value of the stream function is above the horizontal line $\phi = 0°$.

These effects are a direct consequence of the greater role of the buoyant forces for this case. The stronger secondary flows increase the heat transfer in the upper part of the tube and create an 'asymmetry' for the streamlines.

A direct comparison between the present work and previous numerical studies is not possible because of differences in the ranges of values for *Gr* and *Re*. However, the general results for the temperature profiles and the streamlines are similar to those found by Hieber [10], Ou and Cheng [8].

Figure 12 represents the axial variation of the quantity v_s/v_m, where v_s is the magnitude of the mean cross-sectional velocity at a given point and v_m is the mean axial velocity at the tube entrance obtained from the volumetric flow-rate. Three locations were chosen and for each of them the ratio between the magnitude of the cross-section velocity and the corresponding axial velocity is plotted. For case 5, the larger values of this ratio found for the first half of the tube length correspond to the higher values of the ratio Gr/Re^2. Also note the large values of this ratio over the upper portion of the tube, indicating substantial secondary flow.

Several tests were also run using a solution of water (40% by weight) and propylene–glycol (60% by weight) as the heat exchanger fluid. This solution has a much larger viscosity and Prandtl number than water for the range of temperatures which was investigated. Figure 13 presents the results for case 7. The numerical calculations are in good agreement (within 8%) with the experimental data. Direct comparison between

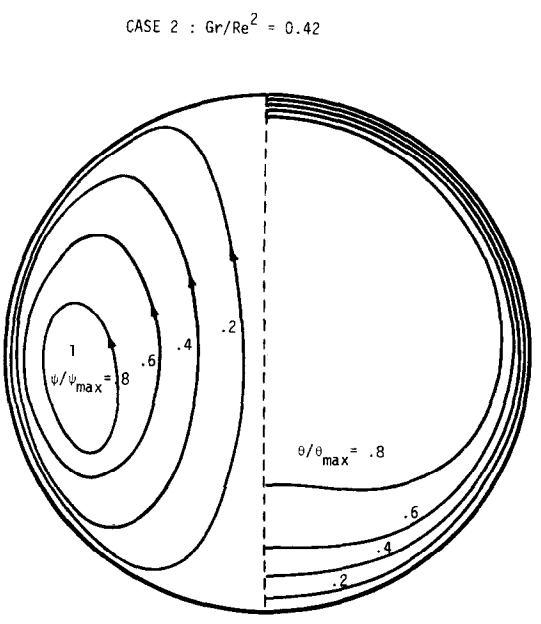

FIG. 10. Streamline and isotherm for $z = L/12$: Case 2 (BC 1; $Ra = 3.2 \times 10^6$; $Re = 1160$).

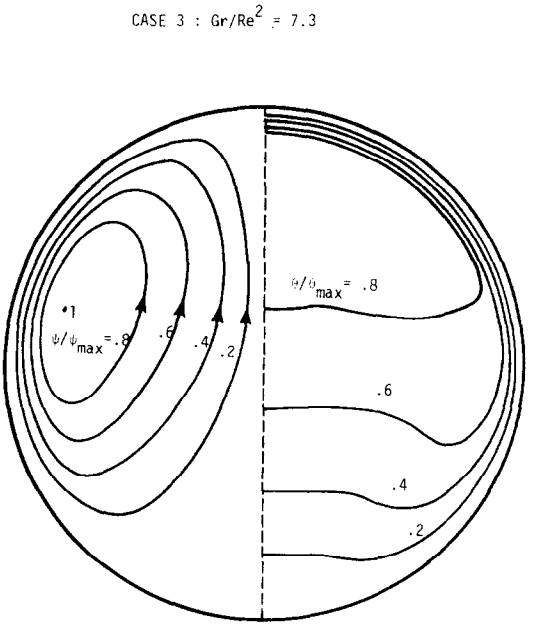

FIG. 11. Streamline and isotherm for $z = L/12$: Case 3 (BC 1; $Ra = 3.5 \times 10^6$; $Re = 298$).

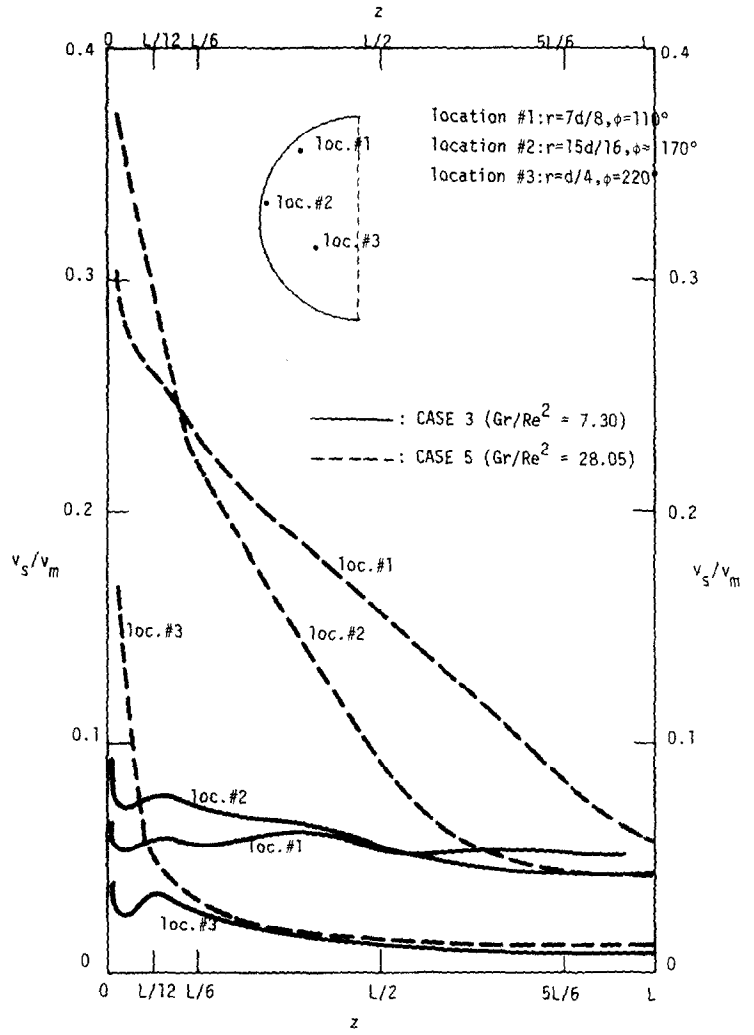

FIG. 12. Ratio between cross-sectional and axial velocities: Case 3 (BC 1; $Ra = 3.5 \times 10^6$; $Re = 298$).

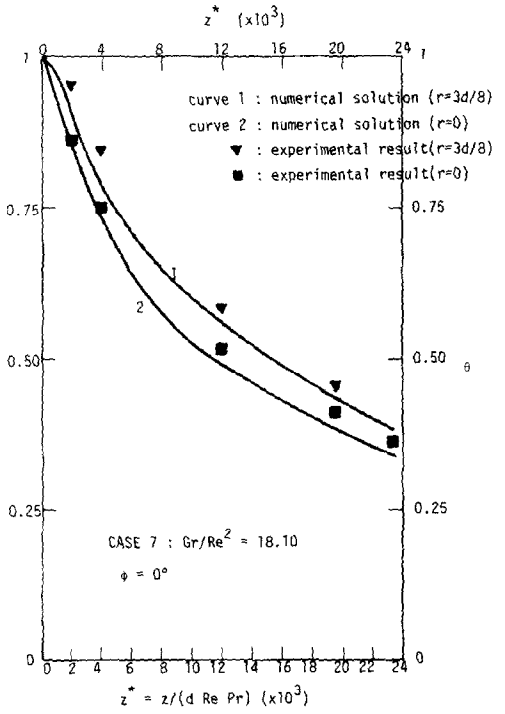

FIG. 13. Dimensionless temperature axial variation (glycol): Case 7 (BC 1; $Ra = 5.5 \times 10^6$; $Re = 104$).

simulations for water and glycol would have required cases having the same characteristic quantity Gr/Re^2. These cases were not specifically studied here.

(E) *Conclusions*

The phenomena resulting from the flow of a buoyant liquid through a short horizontal heat exchanger tube are complex. The natural convection effects within the tube, coupled to the axial motion, create a three-dimensional motion which was studied numerically and experimentally. The flow exhibited strong buoyant forces leading to increased values of the Nusselt number.

In general, the numerical results for the temperature profiles agreed well with the data obtained from the present experiment and also with some earlier numerical studies [7]. The experimental validation of the numerical model for a developing flow was successfully carried out for a number of cases covering a wide range of operating conditions. In this study, the flow was developing throughout the entire length of the short heat exchanger tube. Over the range of conditions tested, the heat transfer in horizontal isothermal tubes was shown to be strongly dependent on secondary flow effects.

REFERENCES

1. E. N. Sieder and G. E. Tate, Heat transfer and pressure drop of liquids in tubes, *Ind. Engng Chem.* **28,** 1429–1436 (1936).
2. A. R. Brown and M. A. Thomas, Combined free and forced convection heat transfer for laminar flow in horizontal tubes, *J. mech. Engng Sci.* **7,** 440–448 (1965).
3. D. G. Kern and D. F. Othmer, Effect of free convection on viscous heat transfer in horizontal tubes, *Trans. Am. Inst. chem. Engrs* **39,** 517–555 (1943).
4. D. R. Oliver, The effect of natural convection on viscous flow heat transfer in horizontal tubes, *Chem. Engng Sci.* **17,** 335–350 (1962).
5. C. A. Depew and S. E. August, Heat transfer due to combined free and forced convection in a horizontal and isothermal tube, *Trans. Am. Soc. mech. Engrs*, Series C, *J. Heat Transfer* **93,** 380–384 (1971).
6. C. A. Hieber, Laminar mixed convection in an isothermal tube: correlation of heat transfer data, *Int. J. Heat Mass Transfer* **25,** 1737–1746 (1982).
7. J. W. Ou and K. C. Cheng, Natural convection effects on the Graetz problem in horizontal isothermal tubes, *Int. J. Heat Mass Transfer* **20,** 953–960 (1977).
8. C. A. Hieber and S. K. Sreenivasan, Mixed convection in an isothermally heated horizontal pipe, *Int. J. Heat Mass Transfer* **17,** 1337–1348 (1974).
9. C. A. Hieber, Mixed convection in an isothermal horizontal tube: some recent theories, *Int. J. Heat Mass Transfer* **24,** 315–322 (1981).
10. A. E. Bergles and R. R. Simonds, Combined forced and free convection for laminar flow in horizontal tubes with uniform heat flux, *Int. J. Heat Mass Transfer* **14,** 1989–2000 (1971).
11. S. T. McComas and E. R. G. Eckert, Combined free and forced convection in a horizontal circular tube, *Trans. Am. Soc. mech. Engrs*, Series C, *J. Heat Transfer* **88,** 147–153 (1966).
12. B. R. Morton, Laminar convection in uniformly heated horizontal pipes at low Rayleigh numbers, *Q. Jl Mech. appl. Math.* **12,** 410–422 (1959).
13. G. N. Faris and R. Viskanta, An analysis of laminar combined forced and free convection heat transfer in a horizontal tube, *Int. J. Heat Mass Transfer* **12,** 1295–1309 (1969).
14. D. P. Siegwarth, R. D. Mikesell, T. C. Readal and T. J. Hanratty, Effect of secondary flow on the temperature field and primary flow in a heated horizontal tube, *Int. J. Heat Mass Transfer* **12,** 1535–1552 (1969).
15. P. H. Newell and A. E. Bergles, Analysis of combined free and forced convection for fully-developed laminar flow in horizontal tubes, *Trans. Am. Soc. mech. Engrs*, Series C, **92,** 83–93 (1970).
16. Y. Mori, K. Futagami, S. Tokuda and M. Nakamura, Forced convective heat transfer in uniformly heated horizontal tubes—1st report: experimental study on the effect of buoyancy, *Int. J. Heat Mass Transfer* **9,** 453–463 (1966).
17. Y. Mori and K. Futagami, Forced convection heat transfer in uniformly heated horizontal tubes—2nd report: theoretical study, *Int. J. Heat Mass Transfer* **10,** 1801–1813 (1967).
18. R. L. Shannon and C. A. Depew, Forced laminar flow convection in a horizontal tube with variable viscosity and free convection effects, *Trans. Am. Soc. mech. Engrs*, Series C, *J. Heat Transfer* **92,** 251–258 (1969).
19. R. L. Shannon and C. A. Depew, Combined free and forced laminar convection in a horizontal tube with uniform heat flux, *Trans. Am. Soc. mech. Engrs*, Series C, *J. Heat Transfer* **90,** 353–357 (1968).
20. S. M. Morcos and A. E. Bergles, Experimental investigation of combined forced and free laminar convection in horizontal tubes, *Trans. Am. Soc. mech. Engrs*, Series C, *J. Heat Transfer* **97,** 212–219 (1965).
21. L. S. Yao, Free-forced convection in the entry region of a heated straight pipe, *J. Heat Transfer* **100,** 202–219 (1978).
22. A. D. Gosman and F. J. K. Ideriah, TEACH-2E: A general computer program for two dimensional, turbulent, recirculating flows, Imperial College, London, and University of California (1983).
23. J. A. C. Humphrey, Numerical calculation of developing laminar flow in pipes of arbitrary curvature radius, *Can. J. chem. Engng* **56,** 151–164 (1978).
24. S. V. Patankar, *Numerical Heat Transfer and Fluid Flow.* McGraw-Hill, New York (1980).
25. A. Lavine, A three-dimensional numerical analysis of fluid flow and heat transfer in a toroidal thermosyphon, Master's thesis, University of California (1983).
26. J. Pascal Coutier, Laminar convection with buoyancy in tube flows with a surrounding liquid medium, Ph.D. thesis, University of California—Berkeley (1983).

APPENDIX A: COMPARISON WITH EXISTING NUSSELT NUMBER CORRELATIONS

The following correlations were studied for the isothermal wall case:

(1) Sieder and Tate (modified):

$$Nu = 1.75(\mu_b/\mu_w)^{0.14} Gz[1 + 0.01\, Gr^{1/3}]$$

(2) Eubank and Proctor:

$$Nu = 1.75(\mu_b/\mu_w)^{0.14}[Gz + 12.6(Gr\, Pr\, D/L)^{0.4}]^{1/3}$$

(3) Oliver:

$$Nu = 1.75(\mu_b/\mu_w)^{0.14}[Gz + 0.00056(Gr\, Pr\, L/D)^{0.7}]^{1/3}$$

(4) Brown and Thomas:

$$Nu = 1.75(\mu_b/\mu_w)^{0.14}[Gz + 0.012(Gz\, Gr^{1/3})^{4/3}]^{1/3}$$

(5) Depew and August:

$$Nu = 1.75(\mu_b/\mu_w)^{0.14}[Gz + 0.12(Gz\, Gr^{1/3}\, Pr^{0.36})^{0.88}]^{1/3}$$

(6) Hieber:

$$(Nu) = (\mu_b/\mu_w)^{0.14}[(\overline{Nu}_B)^3_{lm} + (\overline{Nu}_F)^3_{lm}]^{1/3}$$

with:

$$(\overline{Nu}_B)_{lm} = 2(Gr\, Pr)^{1/4}[\log(1 + 0.4785\sigma_L)]/2.2\sigma_L$$

$$(\overline{Nu}_F)_{lm} = 1.282(2L/D\, Re\, Pr)^{-1/3} \exp(-8.2\, L/D\, Re\, Pr) + 1.828(1 - \exp(-13.5L/D\, Re\, Pr))$$

and

$$\sigma_L = (Gr\, Pr)^{1/4}(2L/D\, Re\, Pr).$$

A manipulation of the correlation by Depew and August leads to the following expression where the term Gr/Re appears:

$$Nu = 1.75(\mu_b/\mu_w)^{0.14}[Gz + 0.12(d/L)^{0.88} Re^{3/2}(Gr/Re^2)^{0.3}]^{1/3}.$$

APPENDIX B: DESCRIPTION OF 'TOROID'

Treatment of the conservation equations

The basic equation solved by the program is of the form:

$$\rho(u \cdot \nabla)\psi = \Gamma \nabla^2 \psi + S$$

where ψ is the dependent variable for the conservation equation, Γ is the diffusion coefficient, and S is the 'source term'.

The equations are discretized using the hybrid differencing scheme described in ref. [22]:

$$\sum_{nb} a_{nb}(\psi_{nb} - \psi_p) + S = 0.$$

These equations can be rewritten in the following form:

$$a_p\psi_p = \sum_{nb} a_{nb}\psi_{nb} + S_c$$

where:

$$a_p = \sum_{nb} a_{nb} - S_p.$$

None of these equations contains the pressure distribution. The pressure field must be estimated and placed in the S term. Since the guess is not correct, the mass conservation law is not verified numerically. Therefore the mass conservation equation is transformed into a 'pressure correction equation', which gives correction factors for the velocities and the pressure. This method is called the SIMPLE algorithm method (for Semi-Implicit Method for Pressure Linked Equations) (cf. [22]).

Treatment of the singularity problem at $r = 0$

The difficulty arising from specifying a finite value for the velocities and temperature at the tube center line was originally avoided by offsetting the first radial node slightly from the axis. At that new location, the following conditions were specified:

$$\frac{\partial u}{\partial r} = v = \frac{\partial w}{\partial r} = 0.$$

This did not lead to very accurate results and the following method was used. The first radial node was set exactly on the tube axis. This causes the control volumes near the axis and also the fluxes through the control volume faces to be zero. Thus, the velocities and temperature at the centerline do not have to be specified, since they do not influence the remainder of the flow. The current version of TOROID has one exception to this rule. The control volume for the first calculated radial velocity does not extend all the way to the axis, and therefore does not have a wedge shape. Thus, it is not required to specify the value of the radial velocity at the singularity point. The radial velocity at this point is calculated as the average of the values at the two surrounding nodal points, and the angular velocity is also calculated by this method. The axial velocity and the temperature at the axis are calculated by averaging over all the surrounding values.

ETUDE DE LA CONVECTION MIXTE LAMINAIRE DANS UN TUBE HORIZONTAL AVEC DES CONDITIONS DE PAROI ISOTHERME

Résumé—On étudie expérimentalement et théoriquement l'écoulement laminaire et le transfert de chaleur dans un tube isotherme horizontal. On porte l'attention sur les régimes d'écoulement où l'effet de pesanteur sur l'écoulement forcé est sensible dans le tube. Plusieurs mesures sont conduites dans un large domaine de conditions opératoires avec une solution aqueuse de propylène–glycol dans le tube. Un modèle tridimensionnel est utilisé pour analyser le comportement de l'écoulement et le transfert de chaleur. Les écoulements secondaires créent une grande variation circonférentielle de la température du fluide et du nombre de Nusselt.

UNTERSUCHUNG DER LAMINAREN MISCHKONVEKTION IN EINEM HORIZONTALEN ROHR MIT ISOTHERMEN WANDBEDINGUNGEN

Zusammenfassung—Es werden die laminare Strömung und der Wärmeübergang in einem horizontalen, isothermen Rohr experimentell und theoretisch untersucht. Von besonderem Interesse sind die Strömungsbedingungen, bei denen sich ein Auftriebseffekt auf die erzwungene Strömung im Rohr zeigt. Für ein großes Gebiet der Betriebsparameter wurden mehrere Tests mit Wasser und einer Propylen–Glykol-Lösung im Rohr ausgeführt. Mit einem dreidimensionalen numerischen Modell wurde das Strömungsverhalten und der Wärmeübergang untersucht. Die Sekundärströmungen verursachen eine große Variation der Fluidtemperatur und der Nusselt-Zahl am Umfang.

ИССЛЕДОВАНИЕ ЛАМИНАРНОЙ СМЕШАННОЙ КОНВЕКЦИИ В ГОРИЗОНТАЛЬНОЙ ТРУБЕ ПРИ ИЗОТЕРМИЧЕСКИХ УСЛОВИЯХ НА СТЕНКЕ

Аннотация—Экспериментально и теоретически изучается ламинарное течение и теплоперенос внутри горизонтальной изотермической трубы. Особое внимание уделяется режимам течения, в которых проявляется влияние подъемной силы на вынужденное течение. Проведена серия опытов в широком диапазоне рабочих условий с водой и раствором пропилена–глюколя. Для анализа течения и теплообмена применялась трехмерная численная модель. Вторичные течения приводили к большим изменениям температуры жидкости и числа Нуссельта по периметру трубы.